Keratinocyte-Derived Exosomes in Painful Diabetic Neuropathy

Authors: James Coy-Dibley[1], Nirupa D. Jayaraj[1], Dongjun Ren[2], Paola Pacifico[1], Abdelhak Belmadani[1,2], Yi-Zhi Wang[1], Kamil K. Gebis[1], Jeffrey N. Savas[1], Amy S. Paller[3], Richard J. Miller[2], Daniela M. Menichella[1,2^].

Author affiliation: [1]Department of Neurology, Feinberg School of Medicine, Northwestern University, Chicago, IL, USA, [2]Department of Pharmacology, Feinberg School of Medicine, Northwestern University, Chicago, IL, USA. [3]Department of Dermatology, Feinberg School of Medicine, Northwestern University, Chicago, IL, USA

^ Corresponding author: Daniela Maria Menichella

James Coy-Dibley, MFA

Conflict of interest statement: The authors have declared that no conflict of interest exists.

24 **ABSTRACT**

25 Painful diabetic neuropathy (PDN) is a challenging complication of diabetes with patients

26 experiencing a painful and burning sensation in their extremities. Existing treatments

27 provide limited relief without addressing the underlying mechanisms of the disease. PDN

28 involves the gradual degeneration of nerve fibers in the skin. Keratinocytes, the most

29 abundant epidermal cell type, are closely positioned to cutaneous nerve terminals,

30 suggesting the possibility of bi-directional communication. Exosomes are small

31 extracellular vesicles released from many cell types that mediate cell to cell

32 communication. The role of keratinocyte-derived exosomes (KDEs) in influencing

33 signaling between the skin and cutaneous nerve terminals and their contribution to the

34 genesis of PDN has not been explored. In this study, we characterized KDEs in a well-

35 established high-fat diet (HFD) mouse model of PDN using primary adult mouse

36 keratinocyte cultures. We obtained highly enriched KDEs through size exclusion

37 chromatography and then analyzed their molecular cargo using proteomic analysis and

38 small RNA sequencing. We found significant differences in the protein and microRNA

39 content of HFD KDEs compared to KDEs obtained from control mice on a regular diet

40 (RD), including pathways involved in axon guidance and synaptic transmission.

41 Additionally, using an *in vivo* conditional extracellular vesicle (EV) reporter mouse model,

42 we demonstrated that epidermal-originating GFP-tagged KDEs are retrogradely trafficked

43 into the DRG neuron cell body. Overall, our study presents a potential novel mode of

44 communication between keratinocytes and DRG neurons in the skin, revealing a possible

45 role for KDEs in contributing to the axonal degeneration that underlies neuropathic pain

46 in PDN. Moreover, this study presents potential therapeutic targets in the skin for

47   developing more effective, disease-modifying, and better-tolerated topical interventions

48   for patients suffering from PDN, one of the most common and untreatable peripheral

49   neuropathies.

INTRODUCTION

Diabetes Mellitus is a very prevalent disease with 29.3 million adults living with diabetes and 115.9 million with pre-diabetes[1]. Painful diabetic neuropathy (PDN) is a disabling, intractable, and common syndrome occurring in approximately 25% of diabetics[2-5]. The associated neuropathic pain significantly impacts the quality of life for patients[6]. Despite its prevalence and impact, current therapies for PDN have limited effects in treating pain[7-10], fail to remediate the damage to nerves, and have side effects associated with their systemic administration[10-12]. Therefore, there is an urgent need for better tolerated and more effective therapies for PDN.

PDN is characterized by neuropathic pain associated with dorsal root ganglion (DRG) nociceptor hyperexcitability and the degeneration of the DRG neuron axons that innervate the skin[13,14]. This results in small fiber neuropathy, where there is a loss or retraction of the cutaneous nerves in the skin epidermis[13,14]. A critical barrier to developing effective treatments for PDN is the lack of understanding of the molecular mechanisms leading to neuropathic pain and small fiber neuropathy.

Keratinocytes are the most abundant epidermal cell type. Recent studies have discovered a new role for keratinocytes in mediating innocuous and noxious touch and thermal sensation in healthy skin[15]. Keratinocytes detect touch stimuli in the skin and transmit mechanical information related to pressure and brushing[16,17]. Optogenetic inhibition of keratinocytes in vivo inhibits the responses to noxious mechanical and thermal stimuli[17,18]. There is also evidence that keratinocytes may contribute to persistent neuropathic pain. A study involving the transplantation of human keratinocytes into rodents with transected nerves showed increased excitability of DRG neurons and

4

73 chronic pain *in vivo*[19]. However, the specific role of keratinocytes in PDN has not been

74 widely investigated.

75 The skin is a highly complex biological system. Along with nociceptive DRG

76 neurons, various other neuronal subpopulations terminate in the skin, both in the dermis

77 and the epidermis[5]. Keratinocytes are closely juxtaposed to cutaneous nerve terminals,

78 suggesting that there may be bidirectional communication. Interestingly, in rodents and

79 human skin, cutaneous nerve terminals in the epidermis form synapse-like contacts and

80 also tunnel through keratinocytes, where they form connexin-43 positive gap junctions,

81 enabling direct cellular communication[20,21]. However, the functional implications of such

82 observations remain unclear. One such ubiquitous mode of intercellular communication

83 recently garnering more appreciation in the skin is mediated by extracellular vesicles

84 (EVs).

85 Exosomes, which are small EVs composed of lipids, proteins and nucleic acids[22-

86 25], were initially posited to be involved in removing cellular waste[26]. However, a substantial

87 body of research now suggests a wider role in intercellular communication. Exosomes

88 are released from most cell types and have been linked to several neurogenerative

89 diseases[27,28] and the progression of different cancers[29]. Keratinocyte-derived exosomes

90 (KDEs) have demonstrated their ability to modulate melanocyte pigmentation[30], regulate

91 dermal fibroblast gene expression[31], mediate crosstalk with macrophages in cutaneous

92 wound healing[32] and play a crucial role in dermal immune responses in psoriasis [33,34].

93 And it has been demonstrated that EVs derived from mesenchymal stem cells can directly

94 alter the excitability of DRG nociceptors in mice[35]. The exploration of the role of exosomes

95 in diabetes, however, has primarily focused on adipose tissue and interorgan

96   communication[36-38]. Recent studies have unveiled a potential role for exosomes in

97   impaired wound healing associated with diabetes[39]. Yet, the research on the effects of

98   exosomes on diabetic neuropathy is limited and has been conducted using exosomes

99   isolated from mesenchymal cells[40,41] or Schwann cells[42]. Notably, exosomes isolated from

100 mesenchymal stromal cells have shown promise in ameliorating peripheral neuropathy in

101 a mouse model of diabetes[40]. Conversely, exosomes derived from high glucose-

102 stimulated Schwann cells have been found to promote the development of diabetic

103 neuropathy in mice[42]. A rigorous and comprehensive investigation of keratinocyte-derived

104 exosomes and their role in PDN represents an important, yet understudied frontier in pain

105 and peripheral neuropathy research.

106   Using size exclusion chromatography, we obtained enriched keratinocyte-derived

107 exosomes from mice and performed an unbiased molecular cargo characterization with

108 proteomics and small RNA sequencing. We found that a high-fat diet-induced PDN mouse

109 model significantly altered the protein and microRNA content of keratinocyte-derived

110 exosomes compared to regular diet control mice. This included alterations in pathways

111 involved in axon guidance and synaptic transmission. Additionally, using an *in vivo*

112 conditional EV reporter mouse line, we demonstrated that epidermal-originating GFP-

113 tagged keratinocyte-derived exosomes are retrogradely trafficked into the DRG neuron

114 cell body. Overall, we present evidence that supports keratinocyte-derived exosomes as

115 a novel interaction pathway between epidermal keratinocytes and DRG neurons and that

116 altered cutaneous EV-trafficking may play a functional role in the development of the

117 small fiber neuropathy observed in PDN.

118

RESULTS

Keratinocytes release a diverse population of exosomes. To study keratinocyte-derived exosomes (KDEs), we cultured primary keratinocytes from adult mice as previously described[17,18]. After collecting cell-conditioned medium (CCM), we fractionated the CCM using a 35-nm pore size-exclusion chromatography column as previously described[43] (Figure 1A) and observed a corresponding increasing total protein concentration with each successive fraction (Figure 1B; silver stain). We immunoblotted for known exosome markers and found fractions 2 and 3 were enriched with the exosome-associated cargo markers Alix, Tsg101, and Syntenin-1 as well as the transmembrane tetraspanins CD63 and CD81[23-25,44] while being negative for GM130 and Calnexin, which are Golgi-associated proteins[45] (Figure 1B). Thus, pooled fractions 2 and 3, which represented our highly enriched KDE fractions with minimized free-floating protein contamination, were used for all subsequent analyses[46].

To investigate the role of KDEs in painful diabetic neuropathy, we employed the clinically relevant and well-established high-fat diet (HFD) model of PDN[47-50], where mice are fed either a regular diet (RD) or a diet with a high fat content for ten weeks, during which time they develop obesity, glucose intolerance and mechanical allodynia accompanied with small-fiber degeneration[48-50]. We cultured primary epidermal keratinocytes under the same conditions from RD or HFD mice. At 90% confluency, both RD and HFD cultures expressed keratin-14 (K14), a marker of undifferentiated, basal-layer keratinocytes, and keratin-10 (K10), a marker of differentiated keratinocytes (Supplemental Figure 1A). Additionally, cultured keratinocytes demonstrated a high degree of proliferative ability with Ki67 staining (Supplemental Figure 1B). Interestingly,

142 HFD keratinocytes maintained a phenotype of impaired wound healing after seven days

143 *in vitro* (Supplemental Figure 1C-D), consistent with findings in diabetic patients[51].

144 Fraction 2/3 KDEs were determined to have a size within the range of exosomes of 59.2

145 ± 14.5nm and 70 ± 26.3nm by dynamic light scattering and a concentration peak of 95 ±

146 6.1nm and 86 ± 8.7nm by nanoparticle tracking analysis for RD (Figure 1C-D) and HFD

147 (Supplemental Figure 2B-C), respectively, while TRPS determined that the mean size

148 average for RD KDEs were 97.7 ± 4.5nm with a concentration peak of 72.3 ± 4.5nm

149 (Figure 1E). KDEs from both RD and HFD were visualized via negative staining (Figure

150 1F) and cryo-electron microscopy (Figure 1G), which revealed the expected crescent

151 morphology and intact vesicular structure.

152 **Keratinocytes release soluble factors that encourage DRG neuron axonal growth.**

153 Given that the loss of cutaneous innervation is reported in PDN[13,14,49], we next sought to

154 investigate the role of KDEs on DRG axonal growth. We employed a microfluidics co-

155 culture system with primary adult mouse DRG neurons in one chamber and adult mouse

156 keratinocytes in the other (Figure 2A). This setup allowed for cell medium exchange only

157 through the microchannels between the chambers. Interestingly, we found that DRG

158 neuronal axons crossed the microchannels separating the two chambers at a higher rate

159 when grown in a co-culture with keratinocytes compared to when grown alone, indicating

160 that keratinocytes release soluble growth factors that promote axonal growth (Figure 2B-

161 C).

162 To test whether mouse KDEs are functional, we labeled them with DIR, which is a

163 lipophilic fluorescent dye that binds to lipid membranes, and applied them directly to

164 primary DRG neuron cultures. We observed a robust uptake of these KDEs by both the

165   cell bodies and neurites of the neurons (Figure 2D). To better model physiological

166   relevance, we then cultured DRG neurons in one chamber of our microfluidic system and

167   allowed their neurites to occupy all the microchannels, thus preventing the free flow of

168   medium between chambers. We then added DIR-labeled KDEs to the empty chamber to

169   test whether they could be transported through the neurites to the DRG neuron cell body.

170   Indeed, DIR-labeled KDEs were readily detected in the DRG neuron cell bodies 16 hours

171   post application, suggesting the retrograde transport of DIR-labeled KDEs through the

172   neurites[52] (Figure 2E). We next sought to investigate the cargo of these KDEs.

173   **Keratinocyte-derived exosomes alter their protein cargo in painful diabetic**

174   **neuropathy.** We characterized the KDE protein content in the context of PDN using a

175   proteomic approach[53]. The analysis was performed on the pooled fractions 2/3 using

176   liquid chromatography-tandem mass spectrometry (LC-MS/MS) for both RD and HFD

177   KDEs (Figure 3A). A gene ontology enrichment analysis on proteins detected in pooled

178   fractions 2/3 for both groups clustered in EV categories, suggesting a robust small EV

179   enrichment for both RD and HFD KDEs (Figure 3B). Importantly, we found similar

180   quantities based on the number of spectral counts of the canonical exosome-associated

181   proteins Alix, Tsg101, and Syntenin-1 in both samples (Figure 3C). Interestingly, fractions

182   2/3-enriched proteins also significantly clustered in the GO enrichment term 'Axon

183   Development,' (Figure 3C; Insert), suggesting a neuron-keratinocyte communication

184   pathway via exosomes. Moreover, we identified 128 differentially expressed exosome-

185   associated proteins (EAPs) between RD and HFD KDEs. There were 90 significant EAPs

186   with a fold change (FC) ≥ 1.5 with biological replicates clustering by group (Figure 3D-E).

187   Interestingly, one significant differentially expressed REACTOME pathway that arose was

188   the 'MAPK Family Signaling Cascades,' which included both Mapk1 and Mapk3 (Figure

189   3G left; Adjusted p-value ≤ 0.05), with Mapk1 validated in fraction 2/3 (Figure 3F).

190   Furthermore, a gene ontology enrichment analysis on the EAPs revealed 'Wound Healing'

191   (3G middle; Adjusted p-value ≤ 0.05), which is reported to be impaired in diabetic

192   patients[54] and persisted in our 2D primary HFD keratinocyte cultures (Supplemental

193   Figure 1C-D), as a significant differentially expressed pathway in the HFD KDEs. Notably,

194   several annexins arose, which are reported to play a role in ESCRT-III mediated plasma

195   membrane repair[55-58] and wound healing[55], with annexin VII confirmed in fraction 2/3 on

196   western blot (Figure 3F). As previously reported, DRG nerve afferents have been shown

197   to tunnel through the keratinocyte cytoplasm and form synapse-like contacts[20,21].

198   Interestingly, a differentially expressed pathway that arose was the GO term

199   'Neurotransmitter Secretion' (Figure 3G right; Adjusted p-value ≤ 0.05). These provide

200   compelling evidence of the neuron-keratinocyte communication pathway, which, at least

201   in our system, is altered in a HFD mouse model of PDN. We next sought to further

202   characterize the KDE cargo.

203   **The microRNA cargo of keratinocyte-derived exosomes is altered in painful**

204   **diabetic neuropathy.** Exosomes contain gene-modifying RNAs, with microRNAs being

205   the most abundant RNA species[43]. Several microRNAs have been associated with pain

206   in diabetic neuropathy[59], but the KDE microRNA content has not yet been identified in the

207   context of PDN. Hence, we next investigated the microRNA cargo of RD and HFD KDEs

208   using an unbiased small-library RNA sequencing approach.

209   Interestingly, we found that the top ten most abundant microRNAs identified,

210   including their variants, accounted for 74.8% of the total small RNA sequenced for both

211   groups (Figure 4A). Additionally, the top two hits, the let-7 and miR-23 families, accounted

212   for almost 40% of the total RNA sequenced for both groups. By cross-referencing 3

213   separate databases (Figure 2B), the predicted protein targets of these small RNAs were

214   used to run a KEGG enrichment analysis for let-7 and miR-23, with both revealing 'Axon

215   Guidance' as a predicted target pathway (Figure 4C). Between the RD and HFD KDEs,

216   there were 35 significant differentially expressed microRNAs that clustered by group

217   (Figure 4D) with 33 with a fold change (FC) ≥ 1.5 (Figure 4E). By cross-referencing the

218   same three databases, the predicted target proteins from each microRNA were run

219   through a gene ontology enrichment analysis with three producing significant target

220   pathways (Figure 4F; Supplemental Figure 3F-G). Both miR-684, which has been

221   implicated in multiple sclerosis[60], and miR24-3p, which has been studied in the context of

222   cancers[61,62] along with its regulation of proliferation related to annexin-6 activity[63],

223   revealed predicted target axon-guidance related pathways (Figure 4G), further providing

224   compelling evidence for a neuron-keratinocyte communication pathway via KDEs under

225   both normal physiology and PDN. Given both the proteomic and small RNA sequencing

226   datasets revealed predicted target pathways involved in axon guidance, and that painful

227   diabetic neuropathy is accompanied by peripheral nerve degeneration[49], we next

228   designed an *in vivo* animal model to investigate the interaction between KDEs and DRG

229   neuron afferent fibers.

230   **Epidermal keratinocyte-derived exosomes are fluorescently labeled with CD63-**

231   **emGFP***. We previously showed that, alongside the luminal exosome markers Alix,

232   Syntenin-1, and Tsg101, fraction 2/3 from our keratinocyte CCM consistently

233   immunoblotted for the transmembrane tetraspanins CD63 and CD81[24] (Figure 1B). We

234   employed the commercially available CD63-emGFP fl/fl mouse line (JacksonLaboratory

235   Strain#:036865) and crossed it with K14-Cre mice to generate a K14-CD63-emGFP EV

236   reporter mouse model (Figure 5A) to label exosomes originating from basal layer

237   keratinocytes and their progeny. We visualized a cross-section of skin with K14

238   immunohistochemistry staining and observed robust GFP expression throughout the

239   epidermis of these mice (Figure 5B), confirming basal layer keratinocytes and their

240   progeny express GFP in the epidermis only. Furthermore, we immunoblotted whole

241   epidermis cell lysate and detected both the membrane-bound CD63-GFP fusion protein

242   and soluble GFP (Figure 5C), presumably due to endogenous protein recycling. We next

243   cultured keratinocytes from this EV-reporter mouse. As expected, we observed a strong

244   GFP signal along the outer membrane of these keratinocytes (Figure 5D). We next

245   immunoblotted all ten fractions obtained from CCM of primary keratinocyte cultures for

246   GFP and detected a strong GFP signal, both the fusion and soluble forms, in fractions

247   2/3, which corresponded to our KDE enriched fractions (Figure 5E). Furthermore, isolated

248   GFP-labeled KDEs were functionally internalized by DRG neurons with GFP detected in

249   both the neuron cell bodies and neurites (Supplemental Figure 4A). Given the gene

250   ontology enrichment pathways highlighted from our proteomic and small RNA sequencing

251   experiments, we next sought to better understand the neuron-keratinocyte

252   communication pathway using our EV reporter mouse line.

253   **Epidermal keratinocyte-derived exosomes are retrogradely transported to the DRG**

254   **neuron cell bodies in male and female mice**. We further investigated the *in vivo*

255   conditional EV-reporter mouse, shifting our focus towards the DRGs. Notably, we

256   detected a GFP signal in DRG cross-sections from both RD and HFD EV-reporter mice

12

257   (Figure 6A; Supplemental Figure 4B) and not in WT DRG controls (Figure 6B).

258   Additionally, the cell lysate of K14-CD63-GFP (KCG) DRG neurons immunoblotted for

259   GFP (Figure 6C), further supporting the evidence for the retrograde transport of GFP-

260   positive epidermal exosomes to the DRG neuron cell bodies. We next cultured primary

261   DRG neurons from the EV-reporter mouse model for both RD and HFD. We observed

262   robust GFP expression in both groups (Figure 6D) with no GFP signal in WT controls

263   (Figure 6E). Interestingly, the GFP observed in these primary DRG neuron cultures

264   presented in the same pattern observed in the DIR-labeled exosomes (Figure 2D) and

265   GFP-labeled exosomes (Supplemental Figure 4A) applied to primary DRG cultures,

266   specifically as puncta[46]. Indeed, we detected these puncta in both the neuron cell bodies

267   and along the neurites (Figure 6F). These data strongly suggest that CD63-GFP-positive

268   keratinocyte-derived exosomes are retrogradely transported from the epidermis to DRG

269   neuron cell bodies, representing a novel mode of communication.

13

DISCUSSION

We isolated and characterized keratinocyte-derived exosomes (KDEs) morphologically and molecularly using an unbiased proteomic and small RNA sequencing approach. Our research revealed that KDEs alter their cargo in a mouse model of painful diabetic neuropathy (PDN), and we identified several gene ontology enrichment pathways that were significantly differentially expressed. In both "omic" datasets, neuron-keratinocyte pathways arose as significantly enriched both under normal physiology and in PDN. Additionally, we created a K14-CD63-emGFP extracellular vesicle (EV)-reporter mouse line and observed a GFP signal in the DRG neurons and neurites, suggesting keratinocyte-derived GFP-tagged exosomes are retrogradely trafficked from epidermal keratinocytes into the DRG neurons of mice.

These findings suggest a direct communication pathway between the epidermis and the peripheral nervous system, and that this is altered in our HFD mouse model of PDN. In our microfluidic paradigm, the presence of keratinocytes enhanced neurite outgrowth, indicating they release a soluble factor that encourages this growth (Figure 2A-C). Interestingly, proteomic analysis of our KDEs revealed that they contained several catenin and plexin isoforms (3C; Insert). The canonical WNT-signaling pathway plays a significant role in axon development in the central[64,65] and peripheral[66] nervous systems and has been implicated in Schwann cell-axon communication[67]. Plexins, the surface receptors for semaphorins, are involved in neuron axonal growth and guidance as well as a host of other functions[68-71]. Semaphorin 4C-Plexin-b2 signaling has been reported to be markedly increased in states of persistent pain in mice, and downregulation of this pathway led to the impairment of inflammatory hypersensitivity via the RhoA-ROCK-

14

293   dependent mechanisms[72]. Additionally, Sema3A and Plexin A were reported to be

294   dysregulated in the spinal cord of a HFD model of PDN[73]. To our knowledge, this is the

295   first report of these proteins being present as KDE cargo. Additionally, notch1, which was

296   recently reported to facilitate neuron-to-neuron communication through EVs in the

297   hippocampus of mice[46], was detected in our KDEs for all three biological replicates of

298   both diet groups (3C; Insert), suggesting this mechanism of internalization may also apply

299   to keratinocyte-neuron terminal endings in the skin. Notch-signaling is known to play a

300   prominent role in developing neurons, including in axon guidance[74,75]. Mutations in the

301   Notch-ligand Jagged1 was implicated in the development of peripheral neuropathy in two

302   independent families and confirmed in a mouse model[76]. Thus, Notch-signaling may

303   represent an unexplored, novel communication pathway between keratinocytes and DRG

304   neuron terminal nerve endings.

305   The KDEs from both groups contain differentially expressed synaptotagmin, which

306   is an essential component of the presynaptic vesicle release complex that facilitates

307   vesicle fusion with the plasma membrane[77,78], along with synaptophysin and synapsin-2,

308   both of which are involved in regulating vesicle docking to the inner plasma membrane[79-

309   81] (3G; Right Panel). These proteins have all been previously reported in keratinocytes[82].

310   However, it is still unclear why these proteins are present as KDE cargo and what their

311   function in keratinocyte-to-neuron communication might be. Further experiments are

312   required to validate all these cargo proteins, both in mice and human KDEs, and to

313   investigate their mechanism of action on nerve terminals.

314   Our small RNA sequencing dataset aligned with the proteomic data. The top two

315   most abundant small RNAs, let-7 and miR-23 (Figure 4A), were predicted to target

316 several prominent signaling pathways that overlapped with the proteomic dataset,

317 including MAPK signaling and the WNT signaling pathways (Figure 4C). A recent study

318 has indicated that partially inhibiting p38-MAPK activation in a diabetic neuropathy rat

319 model led to anti-hyperalgesic effects, suggesting a significant role for MAPKs in

320 nociception modulation[83]. KDEs from both our groups contained a diverse range of MAP-

321 kinases (MAPKs), with mapk1 differentially expressed in our HFD model. Both let-7 and

322 miR-23 have been shown to modulate MAPK activity[84,85]. Additionally, two differentially

323 expressed microRNAs suggested altered keratinocyte-to-neuron communication (Figure

324 4F-G). An altered expression of miR-24-3p has been reported in cancer[61,62,86,87] and

325 diabetes[88]. By cross-referencing three separate databases for predicted targets and

326 running a gene ontology enrichment analysis, one predicted pathway for miR-24-3p

327 modulation is plexin-semaphorin activity, and our proteomic dataset suggested plexin-b2

328 as a cargo protein (Figure 3C). However, the precise mechanism by which these

329 microRNAs regulate axon guidance and how they potentially contribute to PDN remain

330 unclear. Further studies are necessary to understand how these microRNAs modulate

331 target proteins and pathways, either directly or indirectly.

332 The DRG transcriptome is substantially altered in PDN[89] resulting in

333 hyperexcitability of the nociceptive neurons that drive neuropathic pain[49,89], presenting a

334 possible druggable system for future therapeutics. In our studies, using an EV-reporter

335 mouse line in which KDEs are labelled with CD63-emGFP (Figure 6A), we detected a

336 GFP signal in the DRG neuron cell bodies and neurites (Figure 6F). This indicates that

337 GFP-containing exosomes originating in the epidermis are retrogradely trafficked into the

338 DRG neuron cell body, where they can, presumably, initiate transcriptional changes due

339 to their cargo. It should be noted that the GFP species detected, at least from our

340 immunoblotting, was the non-fused form of GFP rather than the CD63-GFP fusion form

341 (Figure 6C), but that the soluble GFP was also detected in the epidermis (Figure 5C) and

342 KDE fractions (Figure 5E) in high abundance. It may be that the GFP-tagged exosomes

343 are trafficked to the DRG neurons, where they release their transcription-altering cargo,

344 and subsequently the fusion protein is then degraded into the soluble GFP that we

345 detected in immunoblotting.

346 This study enhances our understanding of the communication between

347 keratinocytes and DRG neurons and reveals a new role for KDEs in possibly promoting

348 axonal degeneration, which underlies neuropathic pain in PDN. As many genes show

349 differential expression in DRG neurons in PDN mice compared to control mice[90], our

350 studies support a novel strategy for treating PDN by focusing on the skin rather than the

351 entire body. One of the challenges with current PDN treatments is their systemic

352 administration and off-target effects[10-12]. Here, we present evidence for a delivery

353 pathway from epidermal keratinocytes to the peripheral nervous system, which could be

354 utilized to develop and deliver improved topical treatments for PDN and other nervous

355 system diseases. Additionally, our investigation into the role of exosome-mediated

356 communication between keratinocytes and DRG neurons has broader implications.

357 Indeed, exosomes hold great promise as novel disease biomarkers, therapeutic agents,

358 and drug delivery systems. This potential extends beyond PDN, laying the groundwork

359 for exploring new avenues in pain and peripheral neuropathy research and treatment.
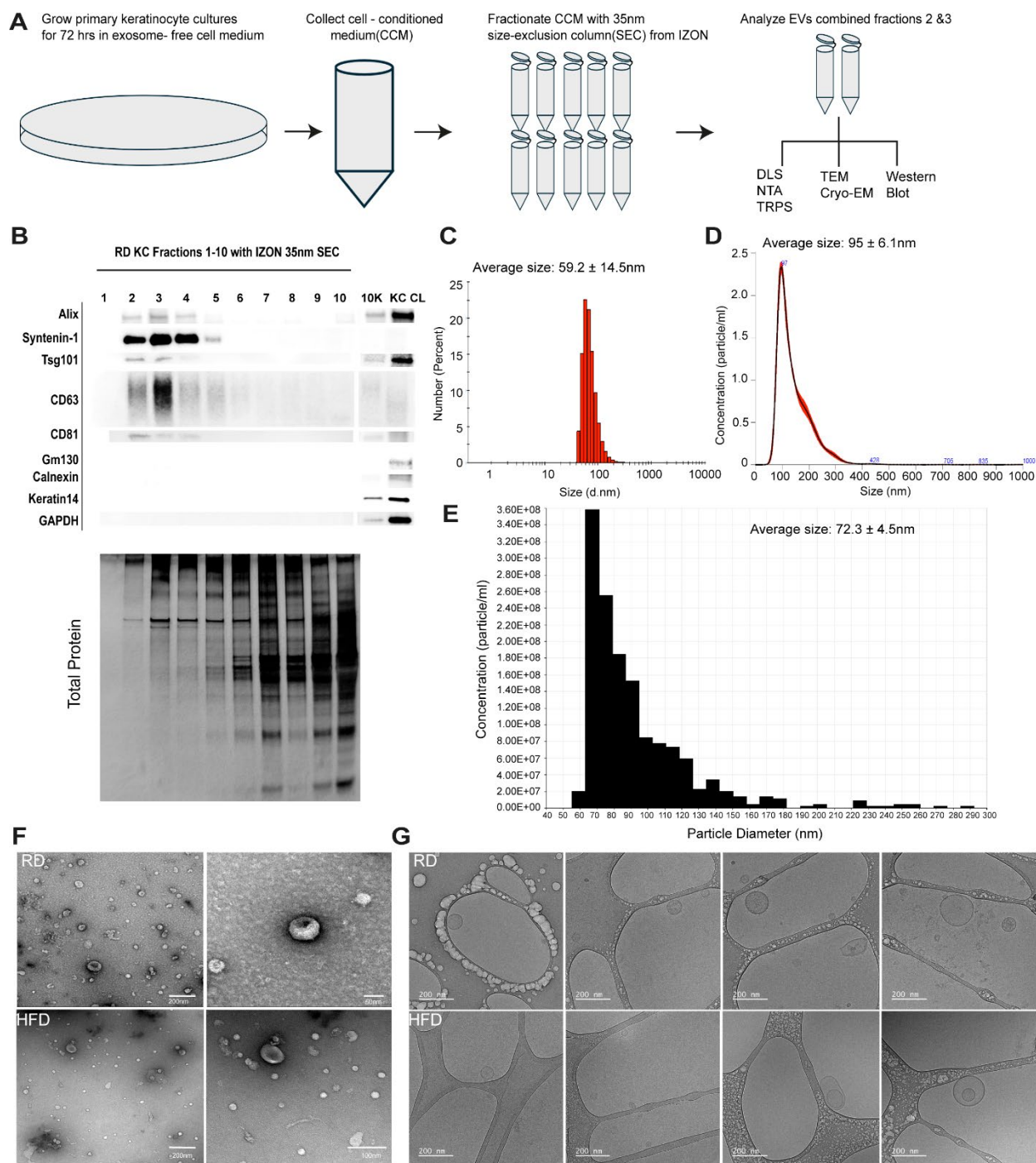
Figure 1: Keratinocytes release a diverse population of exosomes. A) Workflow

schematic for keratinocyte-derived exosome (KDE) isolation using size exclusion

chromatography (SEC). **B)** Immunoblotting the ten SEC fractions revealed exosome-

associated proteins ALIX, Syntenin, Tsg101, CD63 and CD81 were enriched in fractions

364   2 and 3 relative to the total protein concentration (silver stain). **C)** KDEs analyzed with

365   dynamic light scattering had a size range of 59.2 ± 14.5nm (mean ± StDev). N=7

366   across biological replicates from both male and female mice. **D)** KDEs analyzed using

367   nanoparticle tracking analysis produced a concentration peak particle size of 95 ± 6.1

368   nm (mean ± StDev). N=2 male biological replicates. **E)** KDEs analyzed using tunable

369   resistive pulse sensing (TRPS) determined that the mean size average for RD KDEs

370   were 97.7 ± 4.5nm with a concentration peak of 72.3 ± 4.5nm (mean ± StDev). N=3

371   different pressures for one male. **F)** Nanovesicles from combined fraction 2/3 were

372   visualized with negative stain EM. N=11 across 5 biological replicates from male and

373   female mice. **G)** Combined SEC fractions 2/3 were visualized with cryo-EM,

374   demonstrating several diverse populations. N=2 biological replicates, one male and one

375   female.
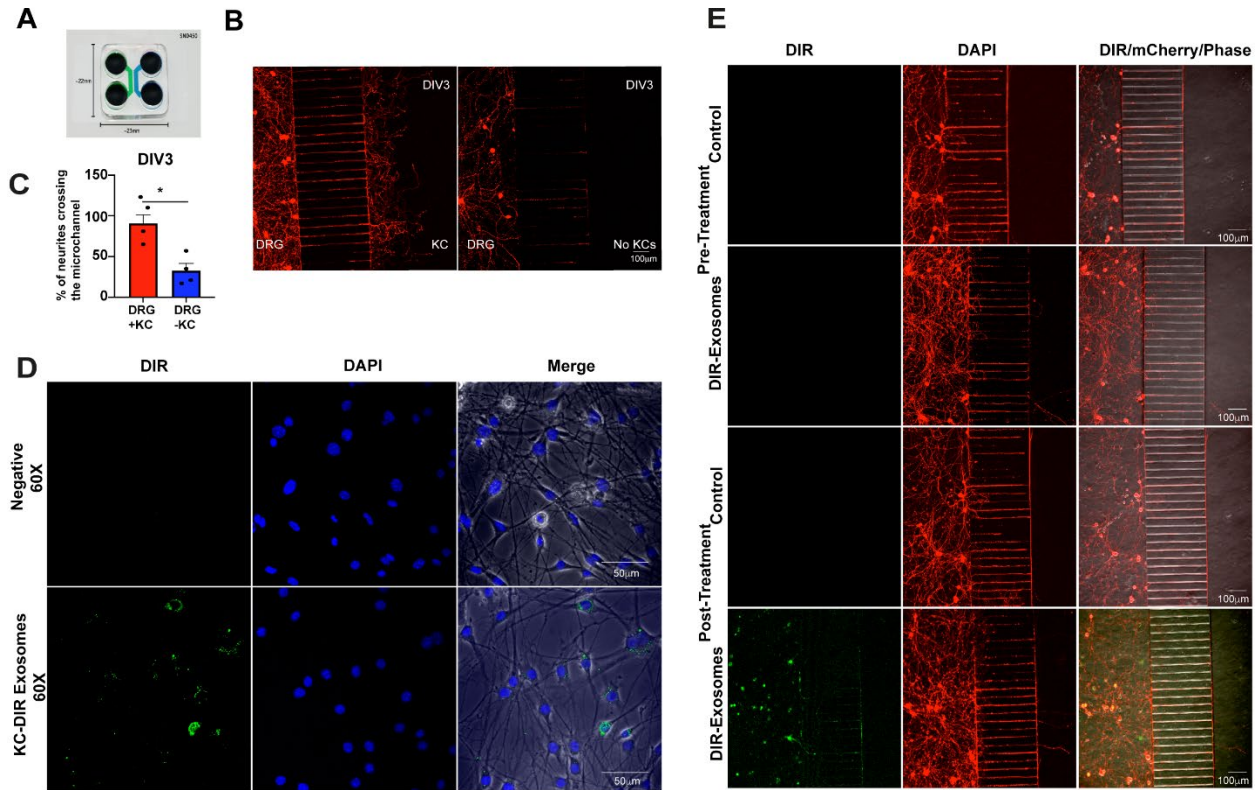
Figure 2: Isolated exosomes from SEC fraction 2/3 are functionally retrogradely trafficked by DRG neurons *in vitro*. A) Representative picture of microfluidics device. **B)** The presence of keratinocytes co-cultured with DRG neurons in a microfluidic paradigm encouraged neurite outgrowth crossing through the microchannels connecting both chambers. **C)** We observed a significant increase in the neurite microchannel crossing when co-cultured in the presence of keratinocytes (p ≤ 0.05, one-tailed, paired t-test; n=5 with KCs and n=4 without KCs paired with DRG primary cultures). **D)** KDEs from SEC Fr2/3 are functionally internalized by primary DRG neurons. N=4 across 2 biological replicates. **E)** KDEs are retrogradely trafficked into the neuron cell body through the neurites in a microfluidic paradigm. N=4 biological replicates.
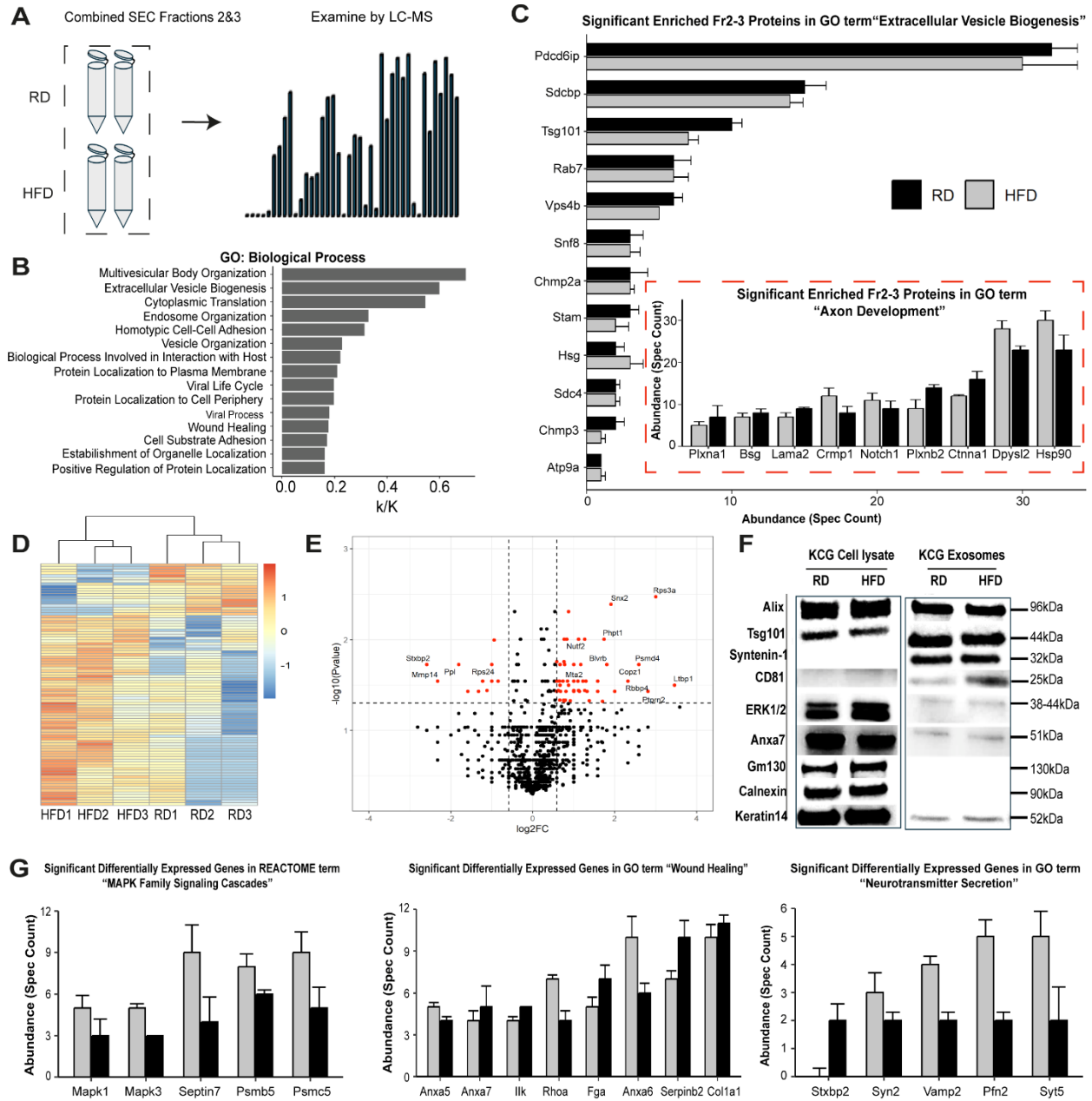
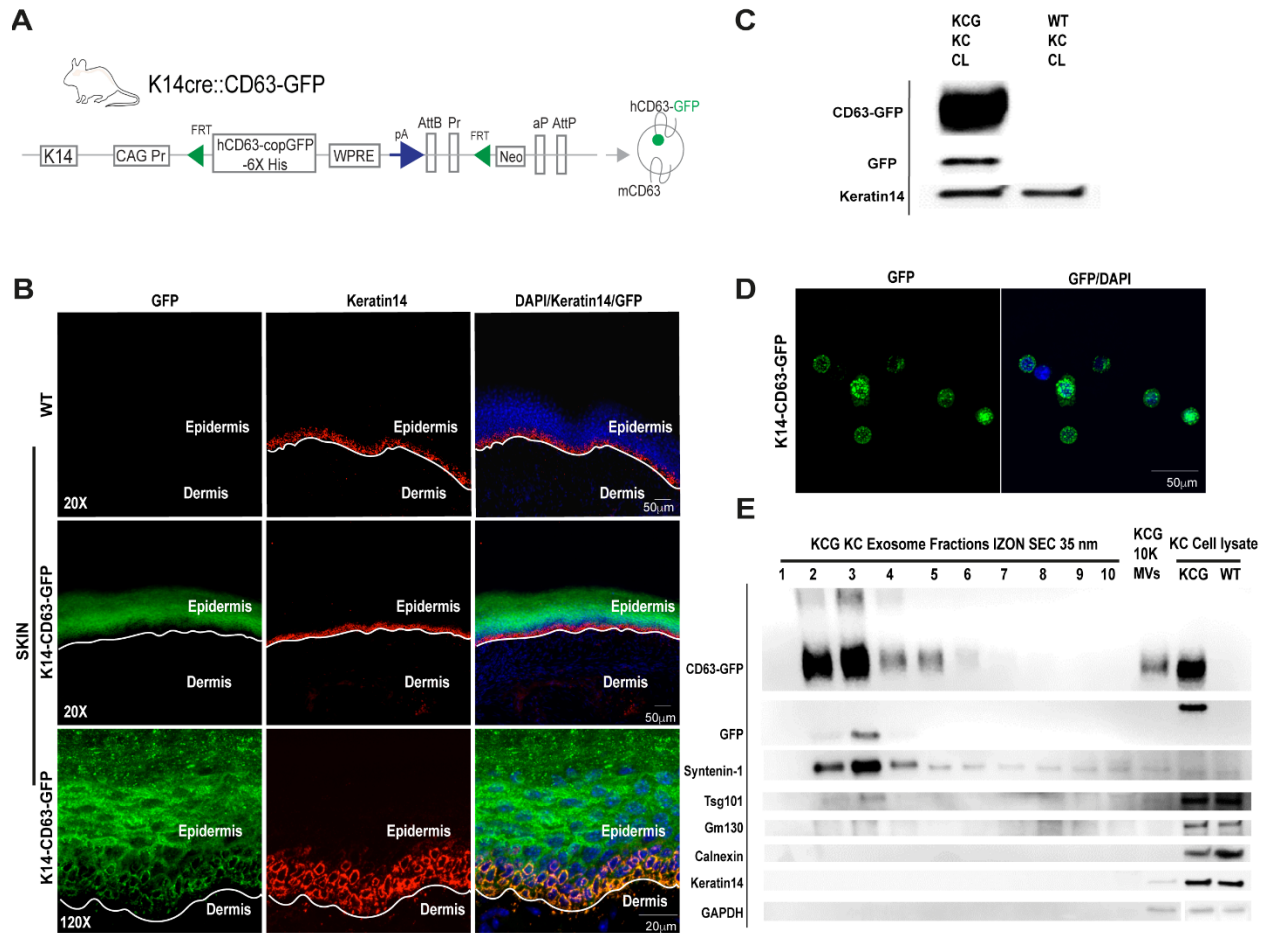**Figure 3: Keratinocyte-derived exosomes (KDEs) significantly alter their protein cargo in painful diabetic neuropathy. A)** Workflow schematic depicting exosome proteomic analysis. N=3 biological replicates for each group from male mice. **B)** The top pathways from a gene ontology enrichment analysis of proteins present in each of the three biological replicates in both experimental groups suggested EV enrichment.

391   Bonferroni adjusted p-value ≤ 0.01. **C)** Select panel of proteins associated with GO Term

392   'EV Biogenesis' revealed similar spectral counts for exosome markers Alix, Syntenin-1,

393   and Tsg101 between both groups. Insert: GO Term 'Axon Development' revealed several

394   unverified notable proteins as exosome cargo. Mean ± SEM. GO Terms Bonferroni

395   adjusted p-value ≤ 0.01. **D)** There were 128 significant differentially expressed exosome-

396   associated proteins (EAPs) (paired t-test, one-way, $p \leq 0.05$) between RD and HFD KDEs.

397   We observed 90 significant EAPs with a ≥ 1.5-fold change (FC) that clustered by group.

398   FC calculated as average HFD/RD spectral count for each protein. **E)** Representative

399   volcano plot with the 128 EAPs. EAPs with an FC ≥ 1.5 are labelled red. **F)** Western blot

400   confirms two EAPs, Mapk1 (via ERK1/2 expression) and annexin-7 in SEC Fr2/3. n=3

401   biological replicates for each group. **G)** Abundances for EAPS in the differentially

402   expressed GO term 'Wound Healing,' 'Neurotransmitter Secretion,' and the REACTOME

403   term 'MAPK Family Signaling Cascades.' Mean ± SEM. Bonferroni adjusted p-value ≤

404   0.01.
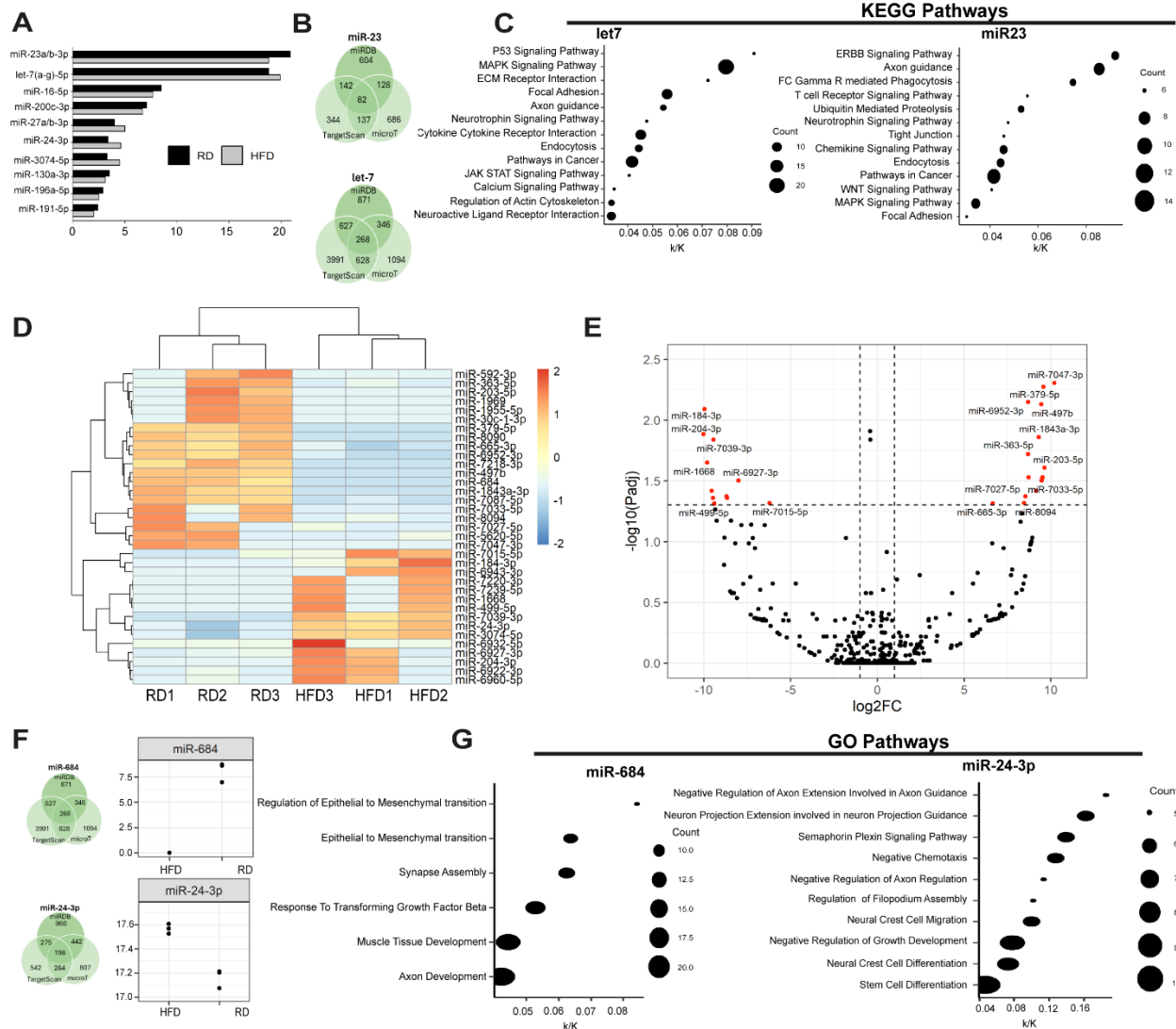
Figure 4: Keratinocyte-derived exosomes (KDEs) alter their small RNA cargo in painful diabetic neuropathy. N=3 biological replicates for male mice in each diet group. A) The top ten small RNAs identified in both RD and HFD KDEs represent 74.8% of the total small RNA sequenced. The top two small RNAs, the let-7 and microRNA-23 families, accounted for almost 40% of the total small RNA sequenced. **B)** The predicted protein targets for let-7 and miR-23 were obtained by cross-referencing 3 separate databases: MirDB, TargetScan, and DIANA-microT. The protein targets predicted by all three programs were used for downstream analysis. **C)** The enrichment analysis of the

413 predicted protein targets of let-7 and miR-23 both revealed predicted KEGG pathways

414 related to 'Axon Guidance,' suggesting a possible role of KDE small RNAs on

415 keratinocyte-to-neuron communication. KEGG pathways Bonferroni adjusted p-value ≤

416 0.01. **D)** There were 35 differentially expressed microRNAs, which clustered by group.

417 Bonferroni adjusted p-value ≤ 0.05. **E)** Of the 35 differentially expressed microRNAs, 33

418 had a fold change ≥ 1.5 between RD and HFD, with 22 overexpressed in HFD. FC is

419 defined as HFDavg/RDavg microRNA counts for each small RNA. Bonferroni adjusted p-

420 value. **F)** miR-684 was downregulated in HFD while miR-24-3p was upregulated. Using

421 the same three databases as Figure 4B, predicted target proteins lists were obtained for

422 each. **G)** The gene ontology enrichment analysis for these predicted proteins presented

423 several interesting GO Terms. Both differentially expressed microRNAs predicted axon-

424 related pathways, further providing evidence for an altered keratinocyte-to-neuron

425 communication via exosome cargo. GO Terms Bonferroni adjusted p-value ≤ 0.01.

Figure 5: Epidermal keratinocyte-derived exosomes (KDEs) are enriched with GFP in an EV-reporter mouse model. A) We created an EV-reporter mouse line by crossing the commercially available CD63-GFP fl/fl mouse line with K14-Cre to create K14-CD63-GFP (KCG) mice. **B)** IHC on cryo-sections of glabrous mouse skin demonstrated GFP expression in all layers of the epidermis with no detectable GFP in the dermis. The GFP signal also co-localized with K14 staining, representing the basal layer of the epidermis. **C)** Immunoblotting revealed robust GFP signal in epidermal cell lysate from our EV-reporter mouse line. **D)** GFP was detected in the primary keratinocyte cultures from our EV-reporter mouse line. **E)** Cell-conditioned medium from KCG keratinocyte cultures was run through IZON 35nm SEC columns. Fraction 2/3 was enriched with CD63-GFP and

436   soluble GFP, supporting that KDEs from primary cultured keratinocytes from our EV-

437   reporter mouse line are tagged with the CD63-GFP fusion protein.
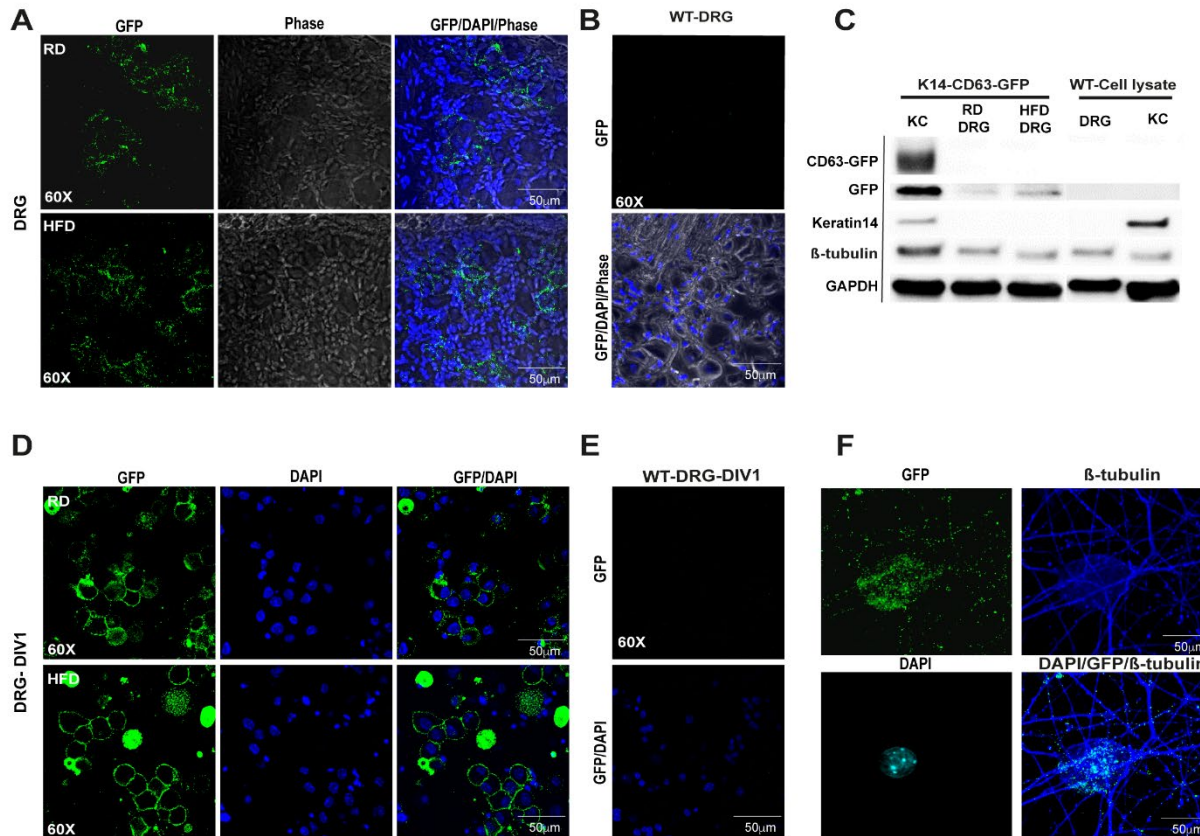
Figure 6: Epidermal keratinocyte-derived exosomes (KDEs) are retrogradely trafficked from the epidermis to DRG neurons *in vivo* in male and female mice. A) We detected GFP signal after immunolabeling amplification in cryosections of the DRGs from the EV-reporter mice for both RD and HFD. N=3 male biological replicates for both RD and HFD and n=2 for RD female mice. **B)** As expected, no false GFP signal was detect in WT DRG cryosections. N=3 biological replicates of WT. **C)** Immunoblotting the DRG cell lysate of EV-reporter mice revealed GFP expression. N=2 biological replicates for both RD and HFD. **D)** We detected GFP signal after IHC amplification in primary DRG cell cultures from the EV-reporter mice for both RD and HFD. N=3 biological replicates for both RD and HFD. **E)** As expected, no false GFP signal was detected in WT primary DRG cultures. N=3 biological replicates of WT. **F)** The GFP signal was not only detected

27

449   in the cell body of the primary DRG cultures from EV-reporter mice but also along the

450   neurites, further providing evidence that KDEs are trafficked along the neurites. N=6

451   biological replicates between RD and HFD.

METHODS

Animals. Animals were housed on a 12-hour light/12-hour dark cycle with ad libitum access to food and water. We used the following mouse lines: K14-Cre, homozygous; CD63-emGFP fl, homozygous; K14-Cre::CD63-emGFP fl heterogenous.

HFD. Mice were fed 42% fat (Envigo TD88137) for 10 weeks as a rodent model of type 2 diabetes. Control mice were fed a regular diet (RD) of 11% fat. After 10 weeks of RD or HFD, a glucose tolerance test was performed as described[49]. A cutoff of (≥140 mg/dl) at 2 SD above the mean for glucose 120 minutes after glucose challenge in WT littermate mice was used as a 'diabetic' classification[49].

Behavioral testing. von Frey behavioral studies were performed as previously described[49] with random experimental group assignments and double-blind investigator and endpoint analysis conditions.

Primary keratinocyte cultures. Glabrous paw skin is dissected from the mouse and incubated in dispase (2.3 mg/ml) overnight. The epidermis is separated from the dermis and incubated in TrypLE Express (10 min, 37C; Gibco 12604-013); the keratinocytes are dislodged using gentle agitation with forceps and then plated on 15cm^2 plates with 154CF epidermal medium (M154CF500) supplemented with 170ul of 0.2M CaCl$_2$ and 5ml of HKGS (S-001-5), which was depleted of EVs following 18 hours of ultracentrifugation at 100,000g. Medium change occurs 24 hours after plating and then every 48 hours. Complete cell culture medium and all other reagents have been confirmed to be EV-free prior to use with the keratinocyte cultures.

Wound healing scratch assay. Primary keratinocyte cultures were grown on 6-well plates (Fisherbrand FB012927) with a 300,000-seeding density and grown to 90%

475   confluency. The tip of an Eppendorf 200ul pipette tip (Fisher 02707409) was used to form

476   a vertical scratch down the center. Cultures were tracked every 24 hours on a Leica 2000

477   LED microscope and analyzed using ImageJ software to measure the rate of gap closure.

478   One-tail paired t-tests were used on the raw dataset to obtain a p-value between groups

479   for each time point (n=58 RD, n=61 HFD for each time point across three separate

480   biological replicates for each group; significance p ≤ 0.05).

481   ***Exosome isolation with size exclusion columns.*** Cell-conditioned medium from

482   keratinocyte cultures is collected between culture confluency of 60-90%, is centrifuged at

483   3000*g* for 30 minutes to remove cell debris and is then concentrated to 500 µl using

484   centrifuge size filters (Pierce Protein Concentrators PES 10K, 88528). The sample is then

485   run through an IZON SEC qEV 35nm column (IZON, ICO-35) as previously reported[43].

486   Fractions 2-3 are used for downstream applications.

487   ***Western Blot.*** Fractions 1-10 of 400ul each are concentrated to 20ul using Millipore

488   centrifuge filters (Microcon 30kDa, MRCF0R030) and combined with one volume

489   equivalent of BioRad 2x Lammalenni loading buffer (BioRad 1610737) with 5% BME.

490   Each fraction is run through a 3-15% gradient gel (BioRad 45610840) alongside full

491   keratinocyte cell lysate (+) and a 10K pellet (large EVs), running a BCA assay (Thermo

492   Scientific) to load ~3 µg of protein per well. Protein was then transferred to PVDF

493   membranes (Millipore) and blocked (BioRad Everyblot 12010020) for 15 minutes. Primary

494   antibodies are applied overnight at 4 °C with secondary antibody at room temperature for

495   2 hours with 3 TBST washes between each step. Proteins are visualized with a

496   chemiluminescence detection system (Thermo Scientific 32209). All western blot gels

497   were run at minimum in triplicate. Blots were visualized on a Li-Cor Odyssey Fc.

498   ***Western blot antibodies.*** The following primary antibodies were used: Alix (Abcam

499   ab88388), Syntenin-1 (Abcam ab19903), Tsg101 (Invitrogen PA531260), CD63

500   (Invitrogen 2H5I1), CD81 (Abcam ab109201), GM130 (Abcam ab52649), Calnexin

501   (Abcam ab22595), K14 (BioLegend 906004), GFP (Abcam ab13970), β-tubulin

502   (ProteinTech 80713-1-RR100UL), GAPDH (Abcam ab181602). The following secondary

503   antibodies were used: Goat anti-rabbit HRP (Abcam ab97080), Goat anti-chicken HRP

504   (Invitrogen A16054).

505   ***Dynamic light scattering.*** 80ul of samples are pipetted into cuvettes (Malvern

506   Catalog#759200) and run through the zetasizer spectrophotometer (Malvern Zetasizer

507   Nano ZSP) with an EV refractive index of 1.35 in ANTEC through Northwestern University.

508   Malvern analytical software is used to analyze the output using particle counts relative to

509   the signal intensity.

510   ***Negative stain EM.*** Samples suspended in PBS are prepared using the standard uranyl

511   acetate fixation for 5 mins seeded on EMS grids (TMS Catalog#71150) and imaged on a

512   FEI Spirit 2 electron microscope. Images were processed using ImageJ software.

513   ***Cryo-EM.*** CryoEM images are obtained through the northwestern BioCryo core facility

514   (NUANCE) with samples prepared as previously described[91].

515   ***Primary DRG Cultures.*** DRG sensory neurons from WT and K14-CD63-GFP mice were

516   dissociated as described[92] at 18 weeks of age.

517   ***Microfluidics.*** Primary DRG cultures were deposited into one compartment chamber

518   connected to the microchannel column in a microfluidic system (XONA Microfluidics

519   SND450) with or without primary keratinocyte cultures in the other compartment

520   chambers. Keratinocytes were cultured for 3 days before depositing DRG cultures unless

521 otherwise specified. The medium was a combination of 50% DRG culture medium as

522 previously described[92] and 50% keratinocyte culture medium when both cell types were

523 present in the chambers.

524 **DIR Labelling.** Concentrated CCM was labeled with DIR (Invitrogen D12731; 2ug/ul) at

525 a ratio of 1:100 by volume and then passed through the IZON 35nm columns. Isolated

526 DIR-labeled exosomes from fractions 2-3 were then used for downstream applications

527 with a negative DIR control, which was DIR-added to concentrated EV-depleted

528 unconditioned medium passed through the column with the same fractions collected for

529 experiments.

530 **DIR-Exosomes**. DRG Cultures: DIR-labeled exosomes were directly applied to DIV-1

531 primary DRG cultures and visualized after 16 hours post-treatment by confocal

532 microscopy. Microfluidics: DIR-exosomes were applied to the empty compartment after

533 DRG neuron neurites occupied all microchannels, preventing medium exchange between

534 the two compartments. The microfluidic chambers were visualized after 16 hours by

535 confocal microscopy.

536 **MS sample preparation**

537 Trichloroacetic acid (TCA, Sigma-Aldrich, Cat# T0699) precipitation was used to clean

538 and precipitate proteins from EV samples. Protein pellets were resuspended in 8 M urea

539 (ThermoFisher Scientific, Cat # 29700) prepared in 100 mM ammonium bicarbonate

540 solution (Fluka, Cat # 09830) and processed with ProteaseMAX (Promega, Cat # V2072)

541 according to the manufacturer's protocol. The samples were reduced with 5 mM Tris(2-

542 carboxyethyl)phosphine (TCEP, Sigma-Aldrich, Cat # C4706; vortexed for 1 hour at RT),

543 alkylated in the dark with 10 mM iodoacetamide (IAA, Sigma-Aldrich, Cat # I1149; 20 min

544   at RT), diluted with 100 mM ABC, and quenched with 25 mM TCEP. Samples were diluted

545   with 100 mM ammonium bicarbonate solution, and digested with Trypsin (1:50, Promega,

546   Cat # V5280) for overnight incubation at 37°C with intensive agitation. The next day,

547   reaction was quenched by adding 1% trifluoroacetic acid (TFA, Fisher Scientific, O4902-

548   100). The samples were desalted using Peptide Desalting Spin Columns (Thermo Fisher

549   Scientific, Cat # 89882). All samples were vacuum centrifuged to dry.

550   ***Tandem Mass spectrometry***

551   Three micrograms of each sample were auto-sampler loaded with a Thermo Vanquish

552   Neo UHPLC system onto a PepMap™ Neo Trap Cartridge (Thermo Fisher Scientific,

553   Cat#: 174500, diameter, 300 µm, length, 5 mm, particle size, 5 □m, pore size, 100 Å,

554   stationary phase, C18) coupled to a nanoViper analytical column (Thermo Fisher

555   Scientific, Cat#: 164570, diameter, 0.075 mm, length, 500 mm, particle size, 3 µm, pore

556   size, 100 Å, stationary phase, C18) with stainless steel emitter tip assembled on the

557   Nanospray Flex Ion Source with a spray voltage of 2000 V. An Orbitrap Ascend (Thermo

558   Fisher Scientific) was used to acquire all the MS spectral data. Buffer A contained 99.9%

559   H_2O and 0.1% FA, and buffer B contained 80.0% ACN, 19.9% H_2O with 0.1% FA. For

560   each fraction, the chromatographic run was for 2 hours in total with the following profile:

561   0-8% for 6, 8% for 64, 24% for 20, 36% for 10, 55% for 10, 95% for 10 and again 95% for

562   6 We used Orbitrap HCD-MS2 method for these experiments. Briefly, ion transfer tube

563   temp = 275 °C, Easy-IC internal mass calibration, default charge state = 2 and cycle time

564   = 3 s. Detector type set to Orbitrap, with 60K resolution, with wide quad isolation, mass

565   range = normal, scan range = 375-1500 m/z, max injection time mode = Auto, AGC target

566   = Standard, microscans = 1, S-lens RF level = 60, without source fragmentation, and

567   datatype = Profile. MIPS was set as on, included charge states = 2-7 (reject unassigned).

568   Dynamic exclusion enabled with n = 1 for 60s exclusion duration at 10 ppm for high and

569   low with Exclude Isotopes. Isolation Mode = Quadrupole, isolation window = 1.6, isolation

570   Offset = Off, active type = HCD, collision energy mode = Fixed, HCD collision energy type

571   = Normalized, HCD collision energy = 25%, detector type = Orbitrap, orbitrap resolution

572   = 15K, mass range = Normal, scan range mode = Auto, max injection time mode = Auto,

573   AGC target = Standard, Microscans = 1, data type = Centroid.mins receptively.

574   ***MS data analysis and quantification***

575   Protein identification/quantification and analysis were performed with Integrated

576   Proteomics Pipeline - IP2 (Bruker, Madison, WI. http://www.integratedproteomics.com/)

577   using ProLuCID[93,94], DTASelect2[95,96], Census and Quantitative Analysis. Spectrum raw

578   files were extracted into MS1, MS2 files using RawConverter

579   (http://fields.scripps.edu/downloads.php). The tandem mass spectra (raw files from the

580   same sample were searched together) were searched against UniProt mouse

581   (downloaded on 07-29-2023) protein databases[97] and matched to sequences using the

582   ProLuCID/SEQUEST algorithm (ProLuCID version 3.1) with 50 ppm peptide mass

583   tolerance for precursor ions and 600 ppm for fragment ions. The search space included

584   all fully and half-tryptic peptide candidates within the mass tolerance window with no-

585   miscleavage constraint, assembled, and filtered with DTASelect2 through IP2. To

586   estimate protein probabilities and false-discovery rates (FDR) accurately, we used a

587   target/decoy database containing the reversed sequences of all the proteins appended

588   to the target database[97] (UniProt, 2015). Each protein identified was required to have a

589   minimum of one peptide of minimal length of six amino acid residues. After the

590   peptide/spectrum matches were filtered, we estimated that the protein FDRs were ≤ 1%

591   for each sample analysis. Resulting protein lists include subset proteins to allow for

592   consideration of all possible protein isoforms implicated by at least three given peptides

593   identified from the complex protein mixtures. Then, we used Census and Quantitative

594   Analysis in IP2 for protein quantification. Static modification: 57.02146 C for

595   carbamidomethylation. Quantification was performed by the built-in module in IP2.

596   ***Proteomics Statistics.*** The spectral counts for each protein accession ID for the three

597   RD and HFD biological replicates are used to run a one-tailed, paired t-test for statistical

598   significance. The average spectral counts for RD and HFD were used to obtain a HFD/RD

599   fold change. The volcano plot was generated in R using ggplot2. The heat map was

600   generated using the R package pheatmap. Gene ontology enrichment analyses were

601   generated using the R packages clusterprofiler, msigdbr and ggplot2. GO enrichment

602   analyses used proteins present in all biological replicates of each group only.

603   ***Small RNA sequencing.*** Samples underwent small RNA sequencing through

604   Northwestern's core facilities. Biological triplicate RD and HFD RNA samples were

605   prepared using the total exosome RNA and protein extraction kit from Invitrogen

606   (Invitrogen Catalog#2743605). RNA samples were quantified by Qubit RNA HS assay

607   and the quality was confirmed by Bioanalyzer RNA pico chip assay. Then, 1ng of RNA

608   was used as input for library preparation with NextFlex small RNA-seq kit v4 according to

609   manufacturer's protocol. Each sample was barcoded with a unique index and multiplexed

610   libraries were pooled for sequencing on Novaseq X Plus 10B flowcell using single end

611   50nt mode.

35

RNA sequencing Statistics. Data analysis was carried out in R using the standard workflow of DESeq2 paired with the libraries apeglm and ggplot2 for figure generation. Bonferroni post-hoc adjustment was used for the reported adjusted p-values ≤ 0.05 for significance. Gene ontology enrichment analyses were generated using the R packages clusterprofiler, msigdbr and ggplot2 with Bonferroni post-hoc adjusted P values < 0.05 for significance.

Protein target analysis. The direct or indirect protein targets for each microRNA was predicted using several target prediction programs, including miRDB (http://mirdb.org/)[98], TargetScan v7.0 (http://www.targetscan.org/vert_72/) and DIANA-microT v5.0 (https://bio.tools/DIANA-microT). Only the predicted proteins identified by all 3 programs were included in the subsequent enrichment analyses.

Immunohistochemistry. Glabrous hind paw dermis/epidermis was separated from the paw and whole DRGs (lumber 2-4) were isolated from 18 week old mice and fixed with 4% PFA for 1 hour, 30% sucrose for 1 hour, and then embedded in OCT. Samples were processed as previously described[50] and analyzed by confocal microscopy.

Antibodies. We used the following primary antibodies on DRG sections: GFP (chicken; Abcam ab13970). We used the following antibodies on skin sections: K14 (BioLegend 906004). We used the following antibodies on primary DRG cultures: GFP (Abcam ab13970), β-tubulin (ProteinTech 80713-1-RR100UL). We used the following secondary antibodies: Goat anti-chicken AlexaFluor™-598 (Invitrogen A-11042), goat anti-rabbit AlexaFluor-647 (Invitrogen A32733).

633 ***EV-Reporter Mouse.*** The commercially available CD63-GFP fl/fl mouse line (Jackson

634 Laboratory Strain#:036865) was crossed with K14-Cre mice to generate the EV-reporter

635 K14-CD63-GFP mouse line.

636 ***Study approval.*** All methods involving animals were approved by the IACUC of

637 Northwestern University.

638

ACKNOWLEDGEMENTS

652

STATEMENT OF DATA AND MATERIALS

654 We will make the raw MS data publicly available in an accessible database upon

655 acceptance.

REFERENCES

1   Martin, S. S. *et al.* 2024 Heart Disease and Stroke Statistics: A Report of US and Global Data From the American Heart Association. *Circulation* **149**, e347-e913 (2024). https://doi.org/10.1161/CIR.0000000000001209

2   American Diabetes, A. Diagnosis and classification of diabetes mellitus. *Diabetes care* **34 Suppl 1**, S62-69 (2011). https://doi.org/10.2337/dc11-S062

3   Dyck, P. J. *et al.* The Rochester Diabetic Neuropathy Study: design, criteria for types of neuropathy, selection bias, and reproducibility of neuropathic tests. *Neurology* **41**, 799-807 (1991).

4   Spallone, V., Lacerenza, M., Rossi, A., Sicuteri, R. & Marchettini, P. Painful diabetic polyneuropathy: approach to diagnosis and management. *The Clinical journal of pain* **28**, 726-743 (2012). https://doi.org/10.1097/AJP.0b013e318243075c

5   Abbott, C. A., Malik, R. A., van Ross, E. R., Kulkarni, J. & Boulton, A. J. Prevalence and characteristics of painful diabetic neuropathy in a large community-based diabetic population in the U.K. *Diabetes care* **34**, 2220-2224 (2011). https://doi.org/10.2337/dc11-1108

6   daCosta DiBonaventura, M., Cappelleri, J. C. & Joshi, A. V. A longitudinal assessment of painful diabetic peripheral neuropathy on health status, productivity, and health care utilization and cost. *Pain medicine* **12**, 118-126 (2011). https://doi.org/10.1111/j.1526-4637.2010.01012.x

7   Bril, V. *et al.* Evidence-based guideline: Treatment of painful diabetic neuropathy: report of the American Academy of Neurology, the American Association of Neuromuscular and Electrodiagnostic Medicine, and the American Academy of Physical Medicine and Rehabilitation. *Neurology* **76**, 1758-1765 (2011). https://doi.org/10.1212/WNL.0b013e3182166ebe

8   Quilici, S. *et al.* Meta-analysis of duloxetine vs. pregabalin and gabapentin in the treatment of diabetic peripheral neuropathic pain. *BMC neurology* **9**, 6 (2009). https://doi.org/10.1186/1471-2377-9-6

9   Callaghan, B. C., Cheng, H. T., Stables, C. L., Smith, A. L. & Feldman, E. L. Diabetic neuropathy: clinical manifestations and current treatments. *Lancet Neurol* **11**, 521-534 (2012). https://doi.org/10.1016/S1474-4422(12)70065-0

10   Finnerup, N. B. *et al.* Pharmacotherapy for neuropathic pain in adults: a systematic review and meta-analysis. *Lancet Neurol* **14**, 162-173 (2015). https://doi.org/10.1016/S1474-4422(14)70251-0

11   Attal, N. & Bouhassira, D. Advances in the treatment of neuropathic pain. *Curr Opin Neurol* **34**, 631-637 (2021). https://doi.org/10.1097/WCO.0000000000000980

12   Shinu, P. *et al.* Novel Therapies for the Treatment of Neuropathic Pain: Potential and Pitfalls. *J Clin Med* **11** (2022). https://doi.org/10.3390/jcm11113002

13   Lauria, G. & Devigili, G. Skin biopsy as a diagnostic tool in peripheral neuropathy. *Nat Clin Pract Neurol* **3**, 546-557 (2007). https://doi.org/10.1038/ncpneuro0630

14   Sommer, C. & Lauria, G. Skin biopsy in the management of peripheral neuropathy. *Lancet Neurol* **6**, 632-642 (2007). https://doi.org/10.1016/S1474-4422(07)70172-2

15   Stucky, C. L. & Mikesell, A. R. Cutaneous pain in disorders affecting peripheral nerves. *Neuroscience letters* **765**, 136233 (2021). https://doi.org/10.1016/j.neulet.2021.136233

16   Mikesell, A. R. *et al.* Keratinocyte PIEZO1 modulates cutaneous mechanosensation. *Elife* **11** (2022). https://doi.org/10.7554/eLife.65987

17   Moehring, F. *et al.* Keratinocytes mediate innocuous and noxious touch via ATP-P2X4 signaling. *Elife* **7** (2018). https://doi.org/10.7554/eLife.31684

18   Sadler, K. E., Moehring, F. & Stucky, C. L. Keratinocytes contribute to normal cold and heat sensation. *Elife* **9** (2020). https://doi.org/10.7554/eLife.58625

19   Radtke, C., Vogt, P. M., Devor, M. & Kocsis, J. D. Keratinocytes acting on injured afferents induce extreme neuronal hyperexcitability and chronic pain. *Pain* **148**, 94-102 (2010). https://doi.org/10.1016/j.pain.2009.10.014

20   Talagas, M. *et al.* Keratinocytes Communicate with Sensory Neurons via Synaptic-like Contacts. *Annals of neurology* **88**, 1205-1219 (2020). https://doi.org/10.1002/ana.25912

21   Erbacher, C. *et al.* Interaction of human keratinocytes and nerve fiber terminals at the neuro-cutaneous unit. *Elife* **13** (2024). https://doi.org/10.7554/eLife.77761

22   van Niel, G., D'Angelo, G. & Raposo, G. Shedding light on the cell biology of extracellular vesicles. *Nat Rev Mol Cell Biol* **19**, 213-228 (2018). https://doi.org/10.1038/nrm.2017.125

23   Mathieu, M., Martin-Jaular, L., Lavieu, G. & Thery, C. Specificities of secretion and uptake of exosomes and other extracellular vesicles for cell-to-cell communication. *Nat Cell Biol* **21**, 9-17 (2019). https://doi.org/10.1038/s41556-018-0250-9

24   Gurung, S., Perocheau, D., Touramanidou, L. & Baruteau, J. The exosome journey: from biogenesis to uptake and intracellular signalling. *Cell Commun Signal* **19**, 47 (2021). https://doi.org/10.1186/s12964-021-00730-1

25   Kalluri, R. & LeBleu, V. S. The biology, function, and biomedical applications of exosomes. *Science* **367** (2020). https://doi.org/10.1126/science.aau6977

26   Pan, B. T., Teng, K., Wu, C., Adam, M. & Johnstone, R. M. Electron microscopic evidence for externalization of the transferrin receptor in vesicular form in sheep reticulocytes. *The Journal of cell biology* **101**, 942-948 (1985). https://doi.org/10.1083/jcb.101.3.942

27   Rastogi, S. *et al.* The Evolving Landscape of Exosomes in Neurodegenerative Diseases: Exosomes Characteristics and a Promising Role in Early Diagnosis. *Int J Mol Sci* **22** (2021). https://doi.org/10.3390/ijms22010440

28   Fan, Y., Chen, Z. & Zhang, M. Role of exosomes in the pathogenesis, diagnosis, and treatment of central nervous system diseases. *J Transl Med* **20**, 291 (2022). https://doi.org/10.1186/s12967-022-03493-6

29   Dai, J. *et al.* Exosomes: key players in cancer and potential therapeutic strategy. *Signal Transduct Target Ther* **5**, 145 (2020). https://doi.org/10.1038/s41392-020-00261-0

30   Lo Cicero, A. *et al.* Exosomes released by keratinocytes modulate melanocyte pigmentation. *Nature communications* **6**, 7506 (2015). https://doi.org/10.1038/ncomms8506

31   Nasiri, G., Azarpira, N., Alizadeh, A., Goshtasbi, S. & Tayebi, L. Shedding light on the role of keratinocyte-derived extracellular vesicles on skin-homing cells. *Stem Cell Res Ther* **11**, 421 (2020). https://doi.org/10.1186/s13287-020-01929-8

32   Zhou, X. *et al.* Exosome-Mediated Crosstalk between Keratinocytes and Macrophages in Cutaneous Wound Healing. *ACS Nano* **14**, 12732-12748 (2020). https://doi.org/10.1021/acsnano.0c03064

33   Jiang, M. *et al.* Keratinocyte exosomes activate neutrophils and enhance skin inflammation in psoriasis. *FASEB journal : official publication of the Federation of American Societies for Experimental Biology* **33**, 13241-13253 (2019). https://doi.org/10.1096/fj.201900642R

34   Kotzerke, K. *et al.* Immunostimulatory activity of murine keratinocyte-derived exosomes. *Exp Dermatol* **22**, 650-655 (2013). https://doi.org/10.1111/exd.12230

35   Ai, M. *et al.* Role of Human Mesenchymal Stem Cells and Derived Extracellular Vesicles in Reducing Sensory Neuron Hyperexcitability and Pain Behaviors in Murine Osteoarthritis. *Arthritis Rheumatol* **75**, 352-363 (2023). https://doi.org/10.1002/art.42353

36   Ashrafizadeh, M., Kumar, A. P., Aref, A. R., Zarrabi, A. & Mostafavi, E. Exosomes as Promising Nanostructures in Diabetes Mellitus: From Insulin Sensitivity to Ameliorating Diabetic Complications. *Int J Nanomedicine* **17**, 1229-1253 (2022). https://doi.org/10.2147/IJN.S350250

749 37 Sun, Y. *et al.* Human Mesenchymal Stem Cell Derived Exosomes Alleviate Type 2 Diabetes Mellitus by Reversing Peripheral Insulin Resistance and Relieving beta-Cell Destruction. *ACS Nano* **12**, 7613-7628 (2018). https://doi.org/10.1021/acsnano.7b07643

752 38 He, Q. *et al.* Mesenchymal stem cell-derived exosomes exert ameliorative effects in type 2 diabetes by improving hepatic glucose and lipid metabolism via enhancing autophagy. *Stem Cell Res Ther* **11**, 223 (2020). https://doi.org/10.1186/s13287-020-01731-6

755 39 Wei, P. *et al.* Exosomes derived from human amniotic epithelial cells accelerate diabetic wound healing via PI3K-AKT-mTOR-mediated promotion in angiogenesis and fibroblast function. *Burns Trauma* **8**, tkaa020 (2020). https://doi.org/10.1093/burnst/tkaa020

758 40 Fan, B. *et al.* Mesenchymal stromal cell-derived exosomes ameliorate peripheral neuropathy in a mouse model of diabetes. *Diabetologia* **63**, 431-443 (2020). https://doi.org/10.1007/s00125-019-05043-0

761 41 Ahmed, L. A. & Al-Massri, K. F. Exploring the Role of Mesenchymal Stem Cell-Derived Exosomes in Diabetic and Chemotherapy-Induced Peripheral Neuropathy. *Mol Neurobiol* (2024). https://doi.org/10.1007/s12035-024-03916-z

764 42 Jia, L. *et al.* Exosomes derived from high-glucose-stimulated Schwann cells promote development of diabetic peripheral neuropathy. *FASEB journal : official publication of the Federation of American Societies for Experimental Biology* **32**, fj201800597R (2018). https://doi.org/10.1096/fj.201800597R

768 43 Böing, A. N. *et al.* Single-step isolation of extracellular vesicles by size-exclusion chromatography. *J Extracell Vesicles* **3** (2014). https://doi.org/10.3402/jev.v3.23430

770 44 Arya, S. B., Collie, S. P. & Parent, C. A. The ins-and-outs of exosome biogenesis, secretion, and internalization. *Trends Cell Biol* **34**, 90-108 (2024). https://doi.org/10.1016/j.tcb.2023.06.006

772 45 Théry, C. *et al.* Minimal information for studies of extracellular vesicles 2018 (MISEV2018): a position statement of the International Society for Extracellular Vesicles and update of the MISEV2014 guidelines. *J Extracell Vesicles* **7**, 1535750 (2018). https://doi.org/10.1080/20013078.2018.1535750

776 46 Wang, Y. Z. *et al.* Notch receptor-ligand binding facilitates extracellular vesicle-mediated neuron-to-neuron communication. *Cell Rep* **43**, 113680 (2024). https://doi.org/10.1016/j.celrep.2024.113680

779 47 George, D. S. *et al.* Mitochondrial calcium uniporter deletion prevents painful diabetic neuropathy by restoring mitochondrial morphology and dynamics. *Pain* (2021). https://doi.org/10.1097/j.pain.0000000000002391

782 48 George, D. S. *et al.* The Mas-related G protein-coupled receptor d (Mrgprd) mediates pain hypersensitivity in painful diabetic neuropathy. *Pain* (2024). https://doi.org/10.1097/j.pain.0000000000003120

785 49 Jayaraj, N. D. *et al.* Reducing CXCR4-mediated nociceptor hyperexcitability reverses painful diabetic neuropathy. *The Journal of clinical investigation* **128**, 2205-2225 (2018). https://doi.org/10.1172/JCI92117

788 50 Menichella, D. M. *et al.* CXCR4 chemokine receptor signaling mediates pain in diabetic neuropathy. *Molecular pain* **10**, 42 (2014). https://doi.org/10.1186/1744-8069-10-42

790 51 Nowak, N. C., Menichella, D. M., Miller, R. & Paller, A. S. Cutaneous innervation in impaired diabetic wound healing. *Transl Res* **236**, 87-108 (2021). https://doi.org/10.1016/j.trsl.2021.05.003

792 52 Frühbeis, C. *et al.* Oligodendrocytes support axonal transport and maintenance via exosome secretion. *PLoS Biol* **18**, e3000621 (2020). https://doi.org/10.1371/journal.pbio.3000621

794 53 Graykowski, D. R., Wang, Y. Z., Upadhyay, A. & Savas, J. N. The Dichotomous Role of Extracellular Vesicles in the Central Nervous System. *iScience* **23**, 101456 (2020). https://doi.org/10.1016/j.isci.2020.101456

797 54 Greenhalgh, D. G. Wound healing and diabetes mellitus. *Clin Plast Surg* **30**, 37-45 (2003).
798 https://doi.org/10.1016/s0094-1298(02)00066-4
799 55 Häger, S. C. & Nylandsted, J. Annexins: players of single cell wound healing and regeneration.
800 *Commun Integr Biol* **12**, 162-165 (2019). https://doi.org/10.1080/19420889.2019.1676139
801 56 Creutz, C. E. The annexins and exocytosis. *Science* **258**, 924-931 (1992).
802 https://doi.org/10.1126/science.1439804
803 57 Sønder, S. L. *et al.* Annexin A7 is required for ESCRT III-mediated plasma membrane repair. *Sci Rep*
804 **9**, 6726 (2019). https://doi.org/10.1038/s41598-019-43143-4
805 58 Williams, J. K., Ngo, J. M., Lehman, I. M. & Schekman, R. Annexin A6 mediates calcium-dependent
806 exosome secretion during plasma membrane repair. *Elife* **12** (2023).
807 https://doi.org/10.7554/eLife.86556
808 59 Fan, B., Chopp, M., Zhang, Z. G. & Liu, X. S. Emerging Roles of microRNAs as Biomarkers and
809 Therapeutic Targets for Diabetic Neuropathy. *Front Neurol* **11**, 558758 (2020).
810 https://doi.org/10.3389/fneur.2020.558758
811 60 Ibrahim, H. M., AlZahrani, A., Hanieh, H., Ahmed, E. A. & Thirugnanasambantham, K. MicroRNA-
812 7188-5p and miR-7235 regulates Multiple sclerosis in an experimental mouse model. *Mol*
813 *Immunol* **139**, 157-167 (2021). https://doi.org/10.1016/j.molimm.2021.07.002
814 61 Mukherjee, S., Shelar, B. & Krishna, S. Versatile role of miR-24/24-1*/24-2* expression in cancer
815 and other human diseases. *Am J Transl Res* **14**, 20-54 (2022).
816 62 Cui, M. *et al.* Interactive functions of microRNAs in the miR-23a-27a-24-2 cluster and the potential
817 for targeted therapy in cancer. *J Cell Physiol* **235**, 6-16 (2020). https://doi.org/10.1002/jcp.28958
818 63 Lin, Z. *et al.* miR-24-3p Dominates the Proliferation and Differentiation of Chicken Intramuscular
819 Preadipocytes by Blocking ANXA6 Expression. *Genes (Basel)* **13** (2022).
820 https://doi.org/10.3390/genes13040635
821 64 Herrera, A. *et al.* Neurogenesis redirects β-catenin from adherens junctions to the nucleus to
822 promote axonal growth. *Development* **150** (2023). https://doi.org/10.1242/dev.201651
823 65 Huang, Y. L. *et al.* Inhibition of Wnt/β-catenin signaling attenuates axonal degeneration in models
824 of Parkinson's disease. *Neurochem Int* **159**, 105389 (2022).
825 https://doi.org/10.1016/j.neuint.2022.105389
826 66 Duraikannu, A., Martinez, J. A., Chandrasekhar, A. & Zochodne, D. W. Expression and Manipulation
827 of the APC-β-Catenin Pathway During Peripheral Neuron Regeneration. *Sci Rep* **8**, 13197 (2018).
828 https://doi.org/10.1038/s41598-018-31167-1
829 67 Lewallen, K. A. *et al.* Assessing the role of the cadherin/catenin complex at the Schwann cell-axon
830 interface and in the initiation of myelination. *The Journal of neuroscience : the official journal of*
831 *the Society for Neuroscience* **31**, 3032-3043 (2011). https://doi.org/10.1523/jneurosci.4345-
832 10.2011
833 68 Alto, L. T. & Terman, J. R. Semaphorins and their Signaling Mechanisms. *Methods in molecular*
834 *biology* **1493**, 1-25 (2017). https://doi.org/10.1007/978-1-4939-6448-2_1
835 69 Janssen, B. J. *et al.* Structural basis of semaphorin-plexin signalling. *Nature* **467**, 1118-1122 (2010).
836 https://doi.org/10.1038/nature09468
837 70 Takamatsu, H. & Kumanogoh, A. Diverse roles for semaphorin-plexin signaling in the immune
838 system. *Trends in immunology* **33**, 127-135 (2012). https://doi.org/10.1016/j.it.2012.01.008
839 71 Li, Y. *et al.* Macrophages facilitate peripheral nerve regeneration by organizing regeneration tracks
840 through Plexin-B2. *Genes Dev* **36**, 133-148 (2022). https://doi.org/10.1101/gad.349063.121
841 72 Paldy, E. *et al.* Semaphorin 4C Plexin-B2 signaling in peripheral sensory neurons is pronociceptive
842 in a model of inflammatory pain. *Nature communications* **8**, 176 (2017).
843 https://doi.org/10.1038/s41467-017-00341-w

844 73   Li, J., Liu, H. Q., Li, X. B., Yu, W. J. & Wang, T. Function of Adenosine 2A Receptor in High-Fat Diet-
845   Induced Peripheral Neuropathy. *J Diabetes Res* **2020**, 7856503 (2020).
846   https://doi.org/10.1155/2020/7856503

847 74   Kopan, R. & Ilagan, M. X. The canonical Notch signaling pathway: unfolding the activation
848   mechanism. *Cell* **137**, 216-233 (2009). https://doi.org/10.1016/j.cell.2009.03.045

849 75   Zhang, Y., Lowe, S., Ding, A. Z. & Li, X. Notch-dependent binary fate choice regulates the Netrin
850   pathway to control axon guidance of Drosophila visual projection neurons. *Cell Rep* **42**, 112143
851   (2023). https://doi.org/10.1016/j.celrep.2023.112143

852 76   Sullivan, J. M. *et al.* Dominant mutations of the Notch ligand Jagged1 cause peripheral neuropathy.
853   *The Journal of clinical investigation* **130**, 1506-1512 (2020). https://doi.org/10.1172/jci128152

854 77   Wolfes, A. C. & Dean, C. The diversity of synaptotagmin isoforms. *Curr Opin Neurobiol* **63**, 198-209
855   (2020). https://doi.org/10.1016/j.conb.2020.04.006

856 78   Ullah, N., Maaiden, E. E., Uddin, M. S. & Ashraf, G. M. Synaptotagmin-1: A Multi-Functional Protein
857   that Mediates Vesicle Docking, Priming, and Fusion. *Curr Protein Pept Sci* **22**, 470-478 (2021).
858   https://doi.org/10.2174/1389203722666210325110231

859 79   Thiel, G. Synapsin I, synapsin II, and synaptophysin: marker proteins of synaptic vesicles. *Brain
860   pathology* **3**, 87-95 (1993). https://doi.org/10.1111/j.1750-3639.1993.tb00729.x

861 80   Cesca, F., Baldelli, P., Valtorta, F. & Benfenati, F. The synapsins: key actors of synapse function and
862   plasticity. *Progress in neurobiology* **91**, 313-348 (2010).
863   https://doi.org/10.1016/j.pneurobio.2010.04.006

864 81   Park, D. *et al.* Cooperative function of synaptophysin and synapsin in the generation of synaptic
865   vesicle-like clusters in non-neuronal cells. *Nature communications* **12**, 263 (2021).
866   https://doi.org/10.1038/s41467-020-20462-z

867 82   Talagas, M. Anatomical contacts between sensory neurons and epidermal cells: an unrecognized
868   anatomical network for neuro-immuno-cutaneous crosstalk. *Br J Dermatol* **188**, 176-185 (2023).
869   https://doi.org/10.1093/bjd/ljac066

870 83   Vieira, W. F. *et al.* Anti-hyperalgesic effects of photobiomodulation therapy (904 nm) on
871   streptozotocin-induced diabetic neuropathy imply MAPK pathway and calcium dynamics
872   modulation. *Sci Rep* **12**, 16730 (2022). https://doi.org/10.1038/s41598-022-19947-2

873 84   Aghaee-Bakhtiari, S. H. *et al.* MAPK and JAK/STAT pathways targeted by miR-23a and miR-23b in
874   prostate cancer: computational and in vitro approaches. *Tumour Biol* **36**, 4203-4212 (2015).
875   https://doi.org/10.1007/s13277-015-3057-3

876 85   Perdas, E., Stawski, R., Nowak, D. & Zubrzycka, M. The Role of miRNA in Papillary Thyroid Cancer
877   in the Context of miRNA Let-7 Family. *Int J Mol Sci* **17** (2016).
878   https://doi.org/10.3390/ijms17060909

879 86   Wang, S. *et al.* MicroRNA-24 in Cancer: A Double Side Medal With Opposite Properties. *Front
880   Oncol* **10**, 553714 (2020). https://doi.org/10.3389/fonc.2020.553714

881 87   Lin, Y. *et al.* miR-24-3p stimulates migration, invasion and proliferation of prostate cancer cells by
882   targeting suppressor of cytokine signaling 6. *Int J Clin Exp Pathol* **11**, 1803-1810 (2018).

883 88   Xiang, Y. miR-24 in diabetes. *Oncotarget* **6**, 16816-16817 (2015).
884   https://doi.org/10.18632/oncotarget.4795

885 89   George, D. S. *et al.* A subpopulation of peripheral sensory neurons expressing the Mas-related G
886   Protein-Coupled Receptor d (Mrgprd) generates pain hypersensitivity in painful diabetic
887   neuropathy. *bioRxiv*, 2022.2010.2027.514066 (2022).
888   https://doi.org/10.1101/2022.10.27.514066

889 90   George, D. S. *et al.* The Mas-related G protein-coupled receptor d (Mrgprd) mediates pain
890   hypersensitivity in painful diabetic neuropathy. *Pain* (2023).
891   https://doi.org/10.1097/j.pain.000000000003120

892   91   Asadi, J. *et al.* Enhanced imaging of lipid rich nanoparticles embedded in methylcellulose films for
893   transmission electron microscopy using mixtures of heavy metals. *Micron* **99**, 40-48 (2017).
894   https://doi.org/10.1016/j.micron.2017.03.019
895   92   Menichella, D. M. *et al.* Ganglioside GM3 synthase depletion reverses neuropathic pain and small
896   fiber neuropathy in diet-induced diabetic mice. *Molecular pain* **12** (2016).
897   https://doi.org/10.1177/1744806916666284
898   93   Eng, J. K., McCormack, A. L. & Yates, J. R. An approach to correlate tandem mass spectral data of
899   peptides with amino acid sequences in a protein database. *J Am Soc Mass Spectrom* **5**, 976-989
900   (1994). https://doi.org/10.1016/1044-0305(94)80016-2
901   94   Xu, T. *et al.* ProLuCID: An improved SEQUEST-like algorithm with enhanced sensitivity and
902   specificity. *J Proteomics* **129**, 16-24 (2015). https://doi.org/10.1016/j.jprot.2015.07.001
903   95   Cociorva, D., D, L. T. & Yates, J. R. Validation of tandem mass spectrometry database search results
904   using DTASelect. *Curr Protoc Bioinformatics* **Chapter 13**, Unit 13.14 (2007).
905   https://doi.org/10.1002/0471250953.bi1304s16
906   96   Tabb, D. L., McDonald, W. H. & Yates, J. R., 3rd. DTASelect and Contrast: tools for assembling and
907   comparing protein identifications from shotgun proteomics. *J Proteome Res* **1**, 21-26 (2002).
908   https://doi.org/10.1021/pr015504q
909   97   UniProt: a hub for protein information. *Nucleic Acids Res* **43**, D204-212 (2015).
910   https://doi.org/10.1093/nar/gku989
911   98   Chen, Y. & Wang, X. miRDB: an online database for prediction of functional microRNA targets.
912   *Nucleic Acids Res* **48**, D127-d131 (2020). https://doi.org/10.1093/nar/gkz757